ADVANCING EARTH AND SPACE SCIENCES

JGR Atmospheres

RESEARCH ARTICLE
10.1029/2024JD041780

# On the Timescales of the Response of the Brewer-Dobson Circulation to an Abrupt Quadrupling of $CO_2$

N. Calvo[1,2], R. R. Garcia[2], G. Chiodo[3,4], D. R. Marsh[5], and L. M. Polvani[6,7,8]

[1]Department of Earth Physics and Astrophysics, Universidad Complutense de Madrid (UCM), Madrid, Spain, [2]Atmospheric Chemistry, Observations and Modelling Lab, National Center for Atmosheric Research, Boulder, CO, USA, [3]Institute for Atmospheric and Climate Sciences, ETH Zurich, Zurich, Switzerland, [4]Instituto de Geociencias (IGEO), Consejo Superior de Investigaciones Científicas (CSIC), Madrid, Spain, [5]School of Physics and Astronomy, University of Leeds, Leeds, UK, [6]Department of Applied Physics and Applied Mathematics, Columbia University, New York, NY, USA, [7]Department of Earth and Environmental Sciences, Columbia University, New York, NY, USA, [8]Center for Climate Systems Research, Columbia University, New York, NY, USA

**Key Points:**

- Most of the response of tropical upwelling to an abrupt quadrupling of CO2 occurs on fast timescales (first 2-3 decades after the forcing)
- The tropical upwelling fast response in the shallow branch is driven mainly by changes in the SSTs from the well mixed shallow ocean
- In the deep branch, at 1 hPa, 70% of the fast response in tropical upwelling is due to radiative cooling and 30% to warmer SSTs

**Correspondence to:**

N. Calvo,
nataliac@ucm.es

**Citation:**

Calvo, N., Garcia, R. R., Chiodo, G., Marsh, D. R., & Polvani, L. M. (2025). On the timescales of the response of the Brewer-Dobson circulation to an abrupt quadrupling of $CO_2$. *Journal of Geophysical Research: Atmospheres*, *130*, e2024JD041780. https://doi.org/10.1029/2024JD041780

Received 11 JUN 2024
Accepted 11 JAN 2025

**Author Contributions:**

**Conceptualization:** N. Calvo, R. R. Garcia, D. R. Marsh, L. M. Polvani
**Data curation:** G. Chiodo, D. R. Marsh
**Formal analysis:** N. Calvo
**Investigation:** N. Calvo
**Methodology:** N. Calvo, R. R. Garcia, G. Chiodo, D. R. Marsh
**Software:** N. Calvo
**Writing – original draft:** N. Calvo
**Writing – review & editing:** R. R. Garcia, G. Chiodo, D. R. Marsh, L. M. Polvani

**Abstract** Changes in the Brewer-Dobson circulation (BDC) in response to increasing $CO_2$ concentrations can arise from the direct effect of radiative cooling in the stratosphere or the indirect effects induced by warmer sea surface temperatures (SSTs). This study aims to disentangle these two contributions in the Whole Atmosphere Community Climate Model (WACCM) by analyzing the timescales of the tropical upwelling response to an abrupt quadrupling of $CO_2$. Transient atmosphere-ocean climate model simulations of 100 years under $4xCO_2$ conditions are compared to preindustrial control simulations and to simulations with an atmosphere-only version of WACCM that uses preindustrial SSTs. We find that most of the response in both shallow and deep branches of the BDC occurs on fast timescales (first 2-3 decades). In the shallow branch of the BDC, the response is mainly driven by changes in SSTs in the well-mixed shallow ocean, which cause tropospheric warming and an intensification and upward displacement of the subtropical jets, and alter wave forcing in their vicinity. The contribution from stratospheric radiative cooling is almost negligible. In the upper stratosphere, the response of tropical upwelling begins earlier and develops faster than in the shallow branch, owing to the larger contribution from the rapid adjustments. At 1 hPa, 70% of the fast response relates to stratospheric radiative cooling and 30% to warmer SSTs. The modulation of the filtering of non-orographic gravity waves (mainly of frontal origin) in the subtropics explain most of the response in tropical upwelling in the deep branch, on both fast and slow timescales.

**Plain Language Summary** The Brewer-Dobson circulation (BDC) is the mean meridional circulation in the stratosphere. It comprises two branches: the shallow branch with ascent in the tropics and descent in the subtropics, below about 70 hPa, and the deep branch with ascent in the tropics and descent in the middle and high latitudes. This circulation is key to explain the distribution of temperature and trace gases, such as ozone, in the stratosphere. Climate models predict an acceleration of the BDC with increasing $CO_2$ concentrations, which can occur in two ways: through direct stratospheric cooling or indirect tropospheric warming from warming sea surface temperatures. To separate these two effects, we analyze simulations run with the Whole Atmosphere Community Climate Model (WACCM) in which CO2 concentrations are quadrupled in comparison with preindustrial control simulations. Our results show that most of the response to $4xCO_2$ occurs fast, in the first two to three decades after the forcing. In the shallow branch, this fast response is mainly driven by changes in sea surface temperatures associated with the response of the shallow ocean mixed layer. In the deep branch, the changes occur faster than in the shallow branch, with a dominant contribution of stratospheric cooling in the first 2-3 decades.

## 1. Introduction

The Brewer Dobson circulation (BDC) is the mean meridional circulation of the stratosphere, including both vertical advection by the diabatic or residual-mean circulation and two-way horizontal mixing (e.g., Hall & Plumb, 1994; Plumb et al., 2002). The BDC is responsible for the mean-mass transport from the tropics into the extratropics and thus it is important for the chemical distribution of trace gases in the stratosphere (e.g., water vapor and ozone, Brewer, 1949; Dobson, 1956; Birner & Bönisch, 2011); in this way, it also affects stratospheric thermal structure and radiative heating (Butchart, 2014). Two different branches of the BDC are commonly distinguished: a shallow branch and a deep branch. Although the exact definition of these BDC branches depends on different diagnostics (Birner & Bönisch, 2011; Lin & Fu, 2013), in our study we refer to the shallow branch as that located between about 100 and 70 hPa with its largest upwelling in the tropical lower stratosphere and downwelling in the subtropics and middle latitudes. For the deep branch, located between about 70 and 1 hPa, the upwelling reaches the upper stratosphere and the downwelling extends to the middle and high latitudes of the winter hemisphere.

The BDC has received a lot of attention in the last few decades mainly because of its projected acceleration in response to increasing greenhouse gas concentrations according to general circulation models and chemistry-climate models (e.g., Abalos et al., 2021; Butchart, 2014; Hardiman et al., 2014; Lin & Fu, 2013). This acceleration has important climate implications such as faster removal of CFCs, and modulation of stratospheric ozone recovery (Karpechko et al., 2018), stratosphere-troposphere ozone exchange (Albers et al., 2018) and water vapor entering the stratosphere (Dessler et al., 2013). The projected strengthening of the shallow branch in response to increasing GHGs is consistent with observed changes in temperature, ozone and age of air, and with reanalysis data sets (Arblaster et al., 2014; Garny et al., 2022; Karpechko et al., 2018). In the upper stratosphere, the inter- and intra-model spread in the strengthening of the BDC is large and large uncertainties in the observational trends estimates still remain (Abalos et al., 2021). Garny et al. (2022) concluded that the long-standing discrepancy between models and observational evidence of past BDC trends in the middle and upper stratosphere is not yet resolved.

As the BDC is wave driven, changes in the residual circulation must be related to changes in wave drag. In the lower stratosphere, most modeling studies indicate that explicitly resolved waves are the main driver of the trend in tropical upwelling and that the contribution from parameterized orographic gravity waves is highly model dependent (Abalos et al., 2021; Butchart, 2014; Butchart & Perez-Charlton, 2010). In the middle and upper stratosphere, in addition to changes in resolved wave forcing, changes in parameterized gravity wave drag are key to explaining the projected acceleration of the BDC, although there is little consensus regarding the source of the gravity waves involved or their relative contribution to the total forcing (Abalos et al., 2021; Garcia & Randel, 2008; Oberlander et al., 2013; Palmeiro et al., 2014).

Several studies have been devoted to understanding whether the simulated changes in wave forcing discussed above in response to increasing GHGs come from changes in wave propagation or changes in tropospheric wave generation. Disentangling these two processes is particularly difficult in a free running climate model and, thus, modeling results remain inconclusive. Using WACCM, Garcia and Randel (2008) found a strengthening and upward displacement of the upper flanks of the subtropical jets in the lower stratosphere in response to tropospheric warming as GHG increases. This would cause the critical layers on the equatorward side of the jets to move upward and thus cause larger resolved wave forcing and stronger tropical upwelling (Shepherd & McLandress, 2011). Changes in wave propagation associated with an intensification of the shallow branch were also found by Olsen et al. (2007) and Sigmond et al. (2004). In contrast, Deckert and Dameris (2008) reported enhanced excitation of tropical waves through anomalous convective heating in response to higher sea surface temperatures (SSTs) under climate change. Calvo and Garcia (2009) found both changes in wave generation through changes in latent heat release by tropical convection as well as changes in wave transmission in response to zonal mean wind changes, but the relative importance of each mechanism in driving changes in the shallow branch was different in historical and future climate change simulations. Garny et al. (2011) reported that both mechanisms operated in their simulations, and that changes in wave propagation were more important than changes in wave sources.

To try to isolate further the direct effect of increasing GHGs through radiative forcing in the stratosphere from the indirect effect due to warmer SSTs, simulations with different atmosphere-only CCMs or GCMs have been performed in time-slice mode, that is, without interannual variability in their boundary conditions (Chrysanthou et al., 2020; Garny et al., 2011; Oberlander et al., 2013; Olsen et al., 2007; Oman et al., 2009; Sigmond et al., 2004). They all highlighted the primary role of tropical SST warming in forcing changes in the residual circulation in the lower stratosphere. Sigmond et al. (2004), using the middle atmosphere ECHAM model (MA-ECHAM4), reported that about two thirds of the acceleration of the residual circulation in the lower stratosphere in winter was due to $CO_2$ doubling in the troposphere, including the impact of $CO_2$ on SSTs, and one third to $CO_2$ doubling in the middle atmosphere. Fewer studies have analyzed the forcing agents of the deep branch in the middle and upper stratosphere. Oberlander et al. (2013) and Chrysanthou et al. (2020) analyzed EMAC (ECHAM/

MESSY Atmospheric Chemistry) and HadGEM (Hadley Centre Global Environmental Model) simulations, respectively, and concluded that both warmer SSTs and direct radiative cooling due to increasing GHGs contributed to changes in the deep branch of the BDC. While Oberlander et al. (2013) attributed two thirds of the strengthening of the deep branch to the radiative impact of increasing GHGs and one third to warmer SSTs when comparing A1b GHG conditions in year 2095 with year 2000, Chrysanthou et al. (2020) reported comparable contributions from both effects upon quadrupling $CO_2$ from preindustrial conditions.

In this study, we revisit this topic with a different approach, exploiting the different timescales of the mechanisms responsible for the BDC response that naturally emerge in abrupt quadrupling $CO_2$ experiments. While both radiative forcing and warmer SSTs contribute to changes in the BDC, the former operate on faster timescales than the latter. Contributions from the shallow and deep parts of the ocean would also operate on different time scales. In contrast to previous studies, we use (a) a comprehensive atmosphere-ocean model in order to represent explicitly atmosphere-ocean coupling, and (b) transient simulations to be able to separate fast versus slow responses of the BDC and gain insight into the mechanisms driving the BDC changes under increasing $CO_2$. We analyze additional atmosphere-only simulations, where SSTs are prescribed and do not change, to isolate the dynamical impacts of radiative cooling in the stratosphere and associated rapid adjustments from those arising from the ocean mixed layer. This approach has been used before to understand the response in tropospheric circulation (Ceppi et al., 2018; Grise & Polvani, 2017) and stratospheric ozone (Chiodo et al., 2018) to increased $CO_{2,}$ but it is applied here for the first time to understand the BDC response.

## 2. Model Simulations and Method

We analyzed two sets of simulations performed with different configurations of the Whole Atmosphere Community Climate Model as the atmospheric component of the Community Earth System Model, version 1 (CESM1-WACCM). This model includes atmosphere, ocean, land and sea-ice components. The atmospheric model is coupled to an interactive chemistry module based on version 3 of the Model for Ozone and Related Chemical Tracers (MOZART; Kinnison et al., 2007). Which includes a comprehensive representation of stratospheric chemistry, with more than 200 reactions and 59 advected species. The atmospheric model top is located at about 140 km. The horizontal resolution is 1.9° latitude by 2.5° longitude. None of the integrations used in our study simulates a QBO. Each set of simulations consists of four runs: one canonical pre-industrial control run ("piControl") and three additional runs branched from piControl following an abrupt 4x$CO_2$ increase and differing only in small perturbations of the initial conditions, thus forming a 3-member ensemble.

The first set of simulations was performed with CESM1-WACCM itself, which we have just described. This model configuration is referred to simply as WACCM in what follows. Except for the absence of a QBO, it is nearly identical to the configuration used as part of the Coupled Model Intercomparison Project, Phase 5 (Taylor et al., 2012), whose historical climate was carefully validated by Marsh et al. (2013). The Parallel Ocean Program version 2 (POP2) is used as the ocean component.

The second set of simulations was performed with CESM1-WACCM but without coupled ocean and sea ice components, and will be referred to as WACCMatm. In this later configuration, an annual cycle of climatological sea surface temperatures (SSTs) and sea ice concentrations from 1850 conditions (Rayner et al., 2003) was prescribed as a boundary condition. Identical SSTs are prescribed in the preindustrial and 4x$CO_2$ experiments.

The length of the simulations varies. The piControl simulation with WACCM was run for 200 years, while the piControl simulations performed with the atmosphere-only versions were run for 30 years. The 4x$CO_2$ simulations coupled to an interactive ocean have been run for 100 years and those with prescribed SSTs for 50 years. In all simulation, atmospheric chemistry is interactive, so that composition changes are consistent with $CO_2$ levels. Table 1 summarizes the main characteristics of each set of simulations.

To investigate fast and slow responses of the BDC to an abrupt 4x$CO_2$ forcing, preindustrial control climatologies are defined as the average of the annual-mean of the last 50 years of the integration in WACCM (coupled to the ocean model) and 30 years in WACCMatm. Our analysis is based on annual means following previous studies on changes in the BDC with climate change (e.g., Abalos et al., 2021; Calvo & Garcia, 2009; Garcia & Randel, 2008; Palmeiro et al., 2014). The *fast response* to an abrupt quadrupling of $CO_2$ is defined as the difference between the annual-mean ensemble-mean climatology of years 6–25 in the 4x$CO_2$ simulations and the annual-mean climatology of the piControl simulation as defined above. The first 5 years of the 4x$CO_2$ simulations are not considered

**Table 1**
*WACCM Simulations Used in This Study*

| | | # Ensemble members | Length (yr) | Coupled chemistry | Coupled ocean |
|---|---|---|---|---|---|
| WACCM | piControl | 1 | 200 | YES | YES |
| | $4xCO_2$ | 3 | 100 | YES | YES |
| WACCMatm | piControl | 1 | 30 | YES | NO |
| | $4xCO_2$ | 3 | 50 | YES | NO |

in the computation of the fast response to avoid the fastest changes at the beginning of the perturbed runs and thus be able to calculate a somewhat stationary mean and standard deviation for this period that can be used in statistical tests of mean differences, as discussed below. The *total response* is defined as the average of the annual-mean ensemble mean climatology of years 81–100 minus the annual-mean climatology of the piControl simulation. Finally, the *slow response* is defined as the change between the annual-mean ensemble-mean climatology of years 81–100 (the last 20 years of the integrations) minus the annual-mean ensemble-mean climatology of years 6–25 in the 4xCO2 simulations and therefore is the difference between the *total response* and the *fast response*. Our definition of *fast* and *slow responses* is similar to that chosen in Ceppi et al. (2018) in their analysis of the tropospheric circulation. Our fast response is averaged over a longer period (6–25 instead of 5–10) for the above-mentioned reasons. This is the same length as that used in the fast response in Grise and Polvani (2017) but starting 5 years later (in year 6 instead of year 0 after the forcing). Our slow response is based on years 81–100 instead of 121–140 as used by Ceppi et al. (2018) because our simulations are shorter. Neither the *slow response* nor the *total response* are computed in the perturbed atmosphere-only simulations since these integrations do not include a slow ocean response. These atmosphere-only simulations are run for 50 years only (Table 1).

The robustness of the responses is assessed by a Student's *t*-test of the difference between the means of the relevant periods. Specifically, for the fast response we evaluate the difference between years 6–25 of the WACCM and WACCMatm $4xCO_2$ ensembles and the last 50 years of the WACCM piControl run and 30 years for WACCMatm piControl; for the slow response, we look at the difference between years 81–100 and 6–25 of the WACCM ensemble. Results are considered significant if they exceed the 95% confidence level.

## 3. Results

### 3.1. Response in Tropical Upwelling

Figure 1a shows the WACCM piControl annual-mean climatology of the vertical component of the residual circulation ($\overline{w}^*$) together with the mass streamfunction in a latitude-altitude cross-section. It clearly shows two maxima in tropical upwelling (orange shading), one at around 100 hPa and the other at 1.5 hPa, corresponding respectively to the shallow and deep branches of the residual circulation. Climatological downwelling occurs in the subtropics and middle latitudes for the shallow branch, and at middle and polar latitudes for the deep branch, in agreement with other studies of the BDC in WACCM (e.g., Palmeiro et al., 2014) and in multimodel assessments (Abalos et al., 2021; Hardiman et al., 2014).

The fast and slow responses to the instantaneous quadrupling of $CO_2$ in WACCM can be seen in Figures 1b and 1c. In the fast response (years 6–25 minus piControl), both the shallow and deep branches of the circulation strengthen. In the shallow branch, enhanced tropical upwelling and subtropical downwelling are clearly seen. In the upper stratosphere (deep branch), the fast response consists of an intensification and upward displacement of the tropical upwelling. Note that at high levels the largest response in tropical upwelling appears between 0.8 and 1 hPa while the piControl climatology peaks between 1 and 3 hPa. This upward displacement of the tropical upwelling of the deep branch in WACCM was already noted by Palmeiro et al. (2014), who analyzed BDC changes in transient GHG emission scenarios performed for CMIP. In the extratropics, the fast response consists of an accelerated downwelling in the deep branch, stronger in the NH than in the SH, and reaching lower levels in the NH. The change in the turnaround latitudes (TA, where $\overline{w}^*$ changes sign on a given pressure level, signaling the transition from upwelling and downwelling regions and defining the width of the tropical pipe) is small in the stratosphere. Still, it is consistent with a narrowing of the tropical pipe in the lowermost stratosphere and a widening in the middle and upper stratosphere as reported in previous studies for long-term trends in different climate change scenarios (see, e.g., Abalos et al., 2021; Hardiman et al., 2014; Li et al., 2010; Menzel et al., 2023).

10.1029/2024JD041780

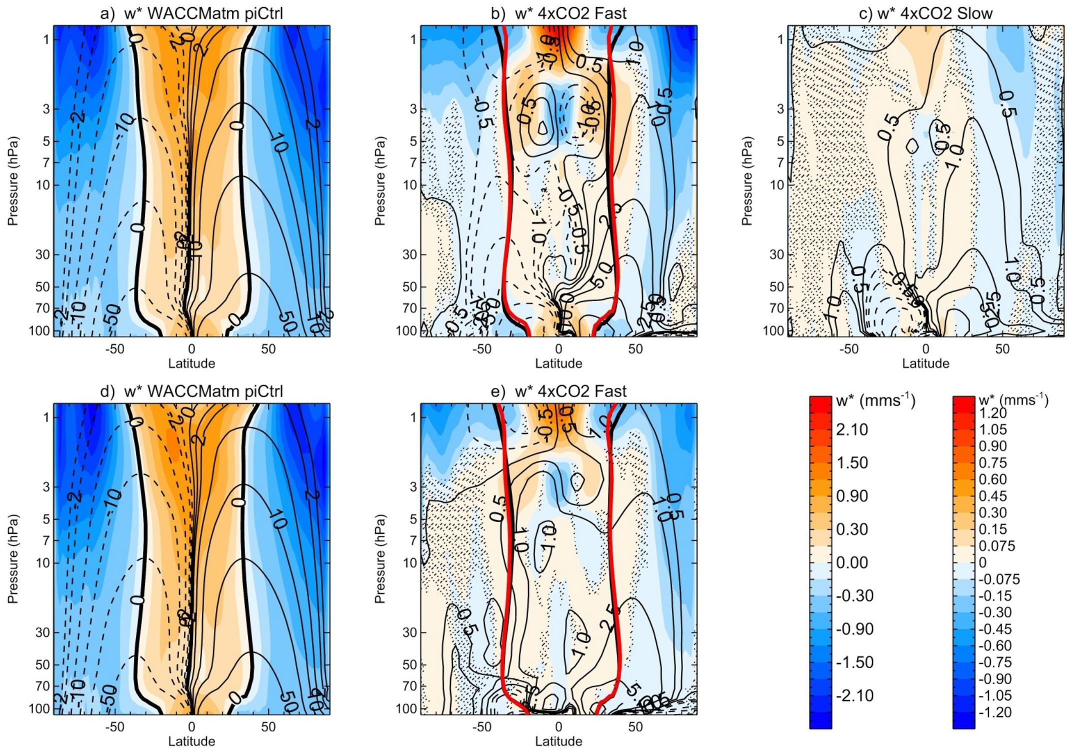


**Figure 1.** Latitude-pressure cross sections of $\overline{w}^*$ (shading) and mass streamfunction (contours) for the preindustrial control climatology (left), the fast response (middle) and the slow response (right). Results for WACCM are shown on the top row and for WACCMatm in the bottom row. TA lats are indicated in black for the piControl climatology, in red for the fast response (years 6–25) and in blue for the final response (years 80–99). Contours for the mass streamfunction are [0, ±1, ±2, ±5, ±10, ±20, ±50] kg m$^{-1}$ s$^{-1}$ for the climatology and half those values for the responses. Shaded contours for $\overline{w}^*$ are drawn at 0, 0.15, 0.3 mm s$^{-1}$ and every 0.3 mm s$^{-1}$ thereafter for the climatology. Contours for the responses are half the values of the climatology. The scales are also indicated by the colorbars, left colorbar for the climatologies, right colorbar for the responses. Dotted areas denotes non significant $\overline{w}^*$ responses at 95% confidence level.

A much more noticeable narrowing of the tropical pipe appears around the stratopause. The fast response in the TA latitudes is of 3.3° in the SH and 3.8° in the NH at 1 hPa. This is due to the intensification of the upwelling in the deep tropics and the weakening (compared to the piControl climatology) in the subtropics.

The slow response (Figure 1c) in the shallow branch is similar in its structure and pattern to the fast response albeit much weaker. As for the deep branch, the slow response in tropical upwelling also consists of an intensification of the climatological pattern, but the response in extratropical downwelling is confined to the NH middle latitudes. Minimal changes in TA latitudes are found in the lower stratosphere in the last 20 years of the simulations compared to those in years 6–25. In the upper stratosphere (at 1 hPa), the change in TA latitudes in the slow response is of 1.8° in the NH and negligible in the SH. Overall, the comparison of fast and slow responses indicates that most of the response to the 4x$CO_2$ increase is dominated by the fast response, occurring already in the first 25 years.

Next, we compare the fast response in WACCM with that in WACCMatm. The piControl climatology in WACCMatm (Figure 1d) is very similar to that in WACCM. Interestingly, the fast response in WACCMatm (Figure 1e) shows very small changes in the lower stratosphere. However, one can see a significant intensification of the deep branch consistent with an upward displacement of the climatological pattern, as in the coupled WACCM simulation but slightly weaker in amplitude, particularly in the tropics and NH polar region. Consistent with the minimal change in $\overline{w}^*$ in the lower stratosphere, no change in the TA latitudes is seen. Above 2 hPa, there is a narrowing of the tropical pipe, consistent with the changes in downwelling, but smaller than in WACCM, mainly related to changes in the northern TA latitude.

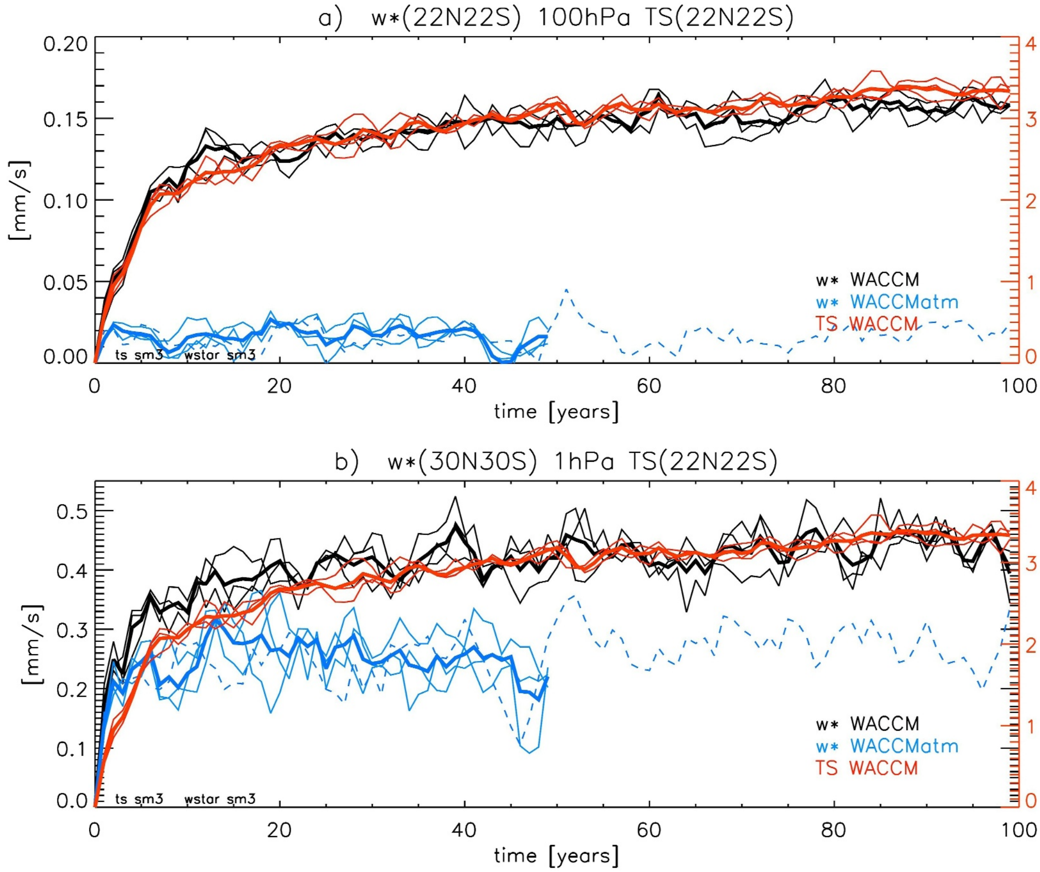


**Figure 2.** Time evolution of the annual mean tropical average of w* at (a) 100 hPa and (b) 1 hPa. Tropical average is defined as ±22° at 100 hPa and ±30° at 1 hPa. Black curves denote WACCM $\overline{w}^*$, and blue curves WACCMatm $\overline{w}^*$. The red curve shows the time evolution of WACCM tropical skin temperature, defined as the average over ±22°. The thin lines indicate individual ensemble members, while the thick lines denote the ensemble mean. The blue dashed curve is the additional 100–years WACCMatm simulation (see text for details). A 3-point smoothing filter has been applied to each curve.

The comparison of the fast $\overline{w}^*$ response in WACCM and WACCMatm gives useful insights into the processes driving the initial BDC response upon quadrupling of $CO_2$. In the shallow branch (cf. Figures 1b and 1e), the response to a 4x$CO_2$ forcing is much larger in the atmosphere-ocean coupled ensemble, indicating that the response is almost entirely driven by the ocean and consequent changes in the SSTs and tropospheric circulation. This implies that a large part of the ocean response already appears on fast timescales (WACCM, years 6–25, Figure 1b), so it must be related to changes in the well-mixed shallow ocean while the response associated with the deep ocean and its large heat capacity, operating on longer timescales, is much weaker (Figure 1c, Yang & Zhu, 2011). In contrast, in the deep branch, the fast response is significant in both WACCM (Figure 1b) and WACCMatm (Figure 1e) but larger in the former, suggesting that the deep branch is driven by both changes in SSTs arising from the ocean's mixed layer and atmospheric radiative adjustments. Changes from the deep ocean, present only in the slow response, also contribute to the total response in the deep branch, albeit to a much lesser extent.

To quantify and visualize the entire evolution of the BDC under 4x$CO_2$ forcing, Figure 2a shows the time series of the annual-mean 4x$CO_2$ response in tropical upwelling at 100 hPa (averaged between 22N and 22S, approximately the TA latitudes at this level) in both WACCM and WACCMatm, together with the response in tropical mean (22N–22S) surface temperature for WACCM simulations. Note that, because the actual SST was not available in the output, we have used instead the model's skin temperature, TS, instead. Over ocean grid cells, TS is equal to SST. The tropical upwelling in the lower stratosphere follows closely the evolution of tropical TS (a similar evolution is obtained when global TS is used). The fast response is 0.122 mm $s^{-1}$ which is 77% of the total response (0.158 mm $s^{-1}$). Indeed, about half of the total response is reached after the first 5 years. In contrast, the response in the WACCMatm simulations is much smaller (mean of 0.016 mm $s^{-1}$ throughout the length of the simulations, which is about 13% of the fast response and 10% of the total response in the WACCM ensemble). This response is reached already within the first year after the 4xCO2 increase. Our results corroborate the dominant role of tropical SSTs in driving the tropical upwelling response of the shallow branch to an abrupt 4x$CO_2$ increase, whereas the contribution of fast atmospheric adjustments is small.

In the upper stratosphere (at 1 hPa, Figure 2b), the behavior is quite different. Note that in this case, the tropical average for $\overline{w}^*$ was computed between 30N and 30S, to account for the broadening of the climatological turn-around latitudes at this level. The results are qualitatively the same when the tropical upwelling is computed between 22N and 22S, which are approximately the limits of the region with positive changes at 1 hPa (see Figures 1b and 1c) or when global TS is used instead of tropical TS. Inspection of Figure 2b shows several important differences compared to the behavior of $\overline{w}^*$ at 100 hPa. First, tropical upwelling does not follow TS as closely as it does at 100 hPa, it responds quicker than TS to the forcing. Second, the response of $\overline{w}^*$ in WACCMatm is about half of the final response in WACCM and no more than 70% of its fast response. These results clearly demonstrate that, in the upper stratosphere, both fast atmospheric radiative adjustments in response to a quadrupling of $CO_2$ and changes in SSTs drive changes in tropical upwelling. As a consequence, the acceleration of $\overline{w}^*$ after the 4x$CO_2$ increase occurs more rapidly in the upper than in the lower stratosphere. Thus, the fast $\overline{w}^*$ response at 1 hPa (0.37 mm $s^{-1}$) accounts for 86% of the final response at that pressure level versus 77% at 100 hPa, consistent with the larger role of fast radiative adjustment in the upper stratosphere. This radiative adjustment takes place immediately after the rapid change in $CO_2$. Indeed, after only 1 year the $\overline{w}^*$ response at 1 hPa reaches about 67% of the total versus 37% at 100 hPa. Consistent with the fast response, the slow response at 1 hPa accounts for only 14% of the total response, which is 60% smaller than its contribution in the shallow branch (at 100 hPa, the contribution of the slow response is 23% of the total). Finally, we note that the evolution of the WACCMatm ensemble through 50 years suggests that there is a slow decrease in $\overline{w}^*$ after about year 15. However, the apparent decrease in $\overline{w}^*$ at 1 hPa in WACCMatm is not statistically significant, as indicated by a *t*-test at the 95% confidence level between years 5–20 and 35–50 in the WACCMatm simulations. To investigate this point further, we carried out an additional WACCMatm simulation covering 100 years (indicated by the blue, dashed curve in Figure 2); it is clear from this simulation that the decrease of $\overline{w}^*$ near year 50 does not continue beyond that time.

As stated in the Introduction, the BDC includes both the residual circulation, described by $\overline{w}^*$ and the streamfunction, and two-way mixing. Mean age of air (AOA) describes the transport of constituents related to these two effects (Hall & Plumb, 1994). Figure 3 shows the annual-mean AOA preindustrial control climatologies and responses to a quadrupling of $CO_2$. Overall, results are consistent with the mass streamfunction shown in Figure 1. Note that changes in AoA are the results of changes in the MMC along the relevant parcel trajectories throughout the stratosphere, and thus, comparisons between changes in the mean-meridional streamfunction and AoA are not straightforward. Figure 3 shows negative fast and slow AOA responses in WACCM, indicative of younger AOA everywhere in the stratosphere and therefore an acceleration of the BDC compared to preindustrial values. The largest change in AOA occurs in the subtropics in the lower stratosphere. Most of the changes occurs in the first decades of the simulation (as fast response) particularly for the shallow branch. In WACCMatm, a small but significant reduction of AOA appears below about 30 hPa, consistent with an intensification of the shallow branch much weaker than in WACCM, as shown in Figure 1. In the middle and upper stratosphere, significant AOA changes in WACCMatm appear in the SH and the tropics, consistent with positive changes (clockwise) in the mass streamfunction and reduced downwelling in the SH middle stratosphere, (Figure 1e), opposite to those in WACCM (Figure 1b). However these changes are small as they account for only 2.5% of their climatological values.

### 3.2. Driving Mechanism of the Tropical Upwelling Response

As mentioned in the Introduction, the residual circulation is wave driven, such that changes in $\overline{w}^*$ can be explained by changes in wave forcing. Wave forcing is closely related to the magnitude and spatial pattern of the zonal-mean zonal winds, which in turn is related to the zonal-mean temperature pattern. Thus, we first examine the changes in these variables in all ensembles, depicted as latitude-pressure cross sections in Figures 4 and 5.

The WACCM ensemble shows a strengthening and upward extension of the subtropical jets in both the fast and slow components of the response (Figures 4b and 4c), which is stronger and extends farther into the midlatitudes

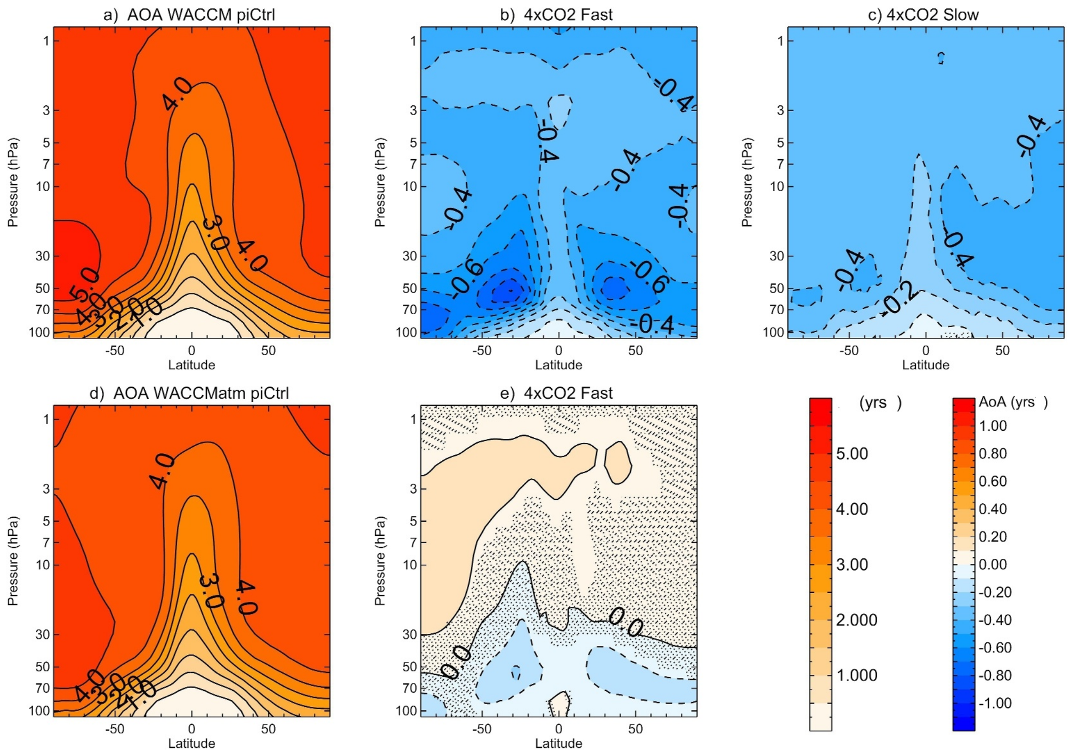


**Figure 3.** As in Figure 1 but for mean age of air (AOA). Units in years. Contours are drawn every 0.5 years for the preindustrial control climatology and every 0.1 years for the responses as indicated in the colorbars. Left colorbar for the climatologies, right colorbar for the responses. Dotted areas denote non-significant responses at the 95% confidence level.

in the fast response. These changes are related to changes in the meridional gradient of temperature in the upper troposphere and lower stratosphere (UTLS) region (Figures 5b and 5c) and do not appear in the fast response in WACCMatm (Figure 4e), consistent with a much weaker tropospheric warming, and a more latitudinally homogeneous temperature response in the UTLS (Figures 5e vs. Figure 5b). It follows that the strengthening of the subtropical jets is driven by the changes in SSTs. This strengthening of the subtropical jets in WACCM is consistent with a small upward and equatorward displacement of the zero-wind lines, as shown in other studies (i.e., Hardiman et al., 2013). In contrast, no change in the zero-wind lines is simulated in WACCMatm. In the SH extratropics, the fast response in both WACCM and WACCMatm exhibits an intensification of the westerly winds in the stratosphere and the troposphere, indicating that these changes are driven by rapid atmospheric adjustments, mainly from stratospheric cooling. Similar changes in zonal mean zonal wind in response to a 4x$CO_2$ increase were reported by Grise and Polvani (2017) for the SH, Ceppi et al. (2018) in the troposphere, and Chrysanthou et al. (2020) in their 50-year time-slice simulations. In addition, the fast and slow responses in WACCM reveal a robust equatorward shift of the stratospheric westerlies in the SH in the middle and upper stratosphere (Figures 4b and 4c) not reported in previous studies. In the NH, an intensification of the stratospheric westerlies appears in WACCM but not in WACCMatm, pointing to the role of the ocean in driving these changes. Interestingly, the slow response (Figure 4c) shows a weakening of the extratropical zonal mean zonal winds significant only in the troposphere and lower stratosphere but not in the middle and upper stratosphere, probably because the changes are smaller than the large internal variability. The warmer polar troposphere near the surface in the NH simulated in all responses is probably related to the amplification effect of changes in the snow cover over Siberia.

Next, we apply the downward control principle (DCP, Haynes et al., 1991) to quantify the contribution of the different waves to changes in tropical upwelling. We follow Palmeiro's et al. (2014) methodology, and we apply the DCP using annual means and the latitude limits that correspond to the annual mean TA latitudes of the piControl climatology. Figure 6 shows the vertical profile of the annual mean tropical upwelling between the TA latitudes, together with the total upwelling computed from the DCP as well as the DCP contribution of the

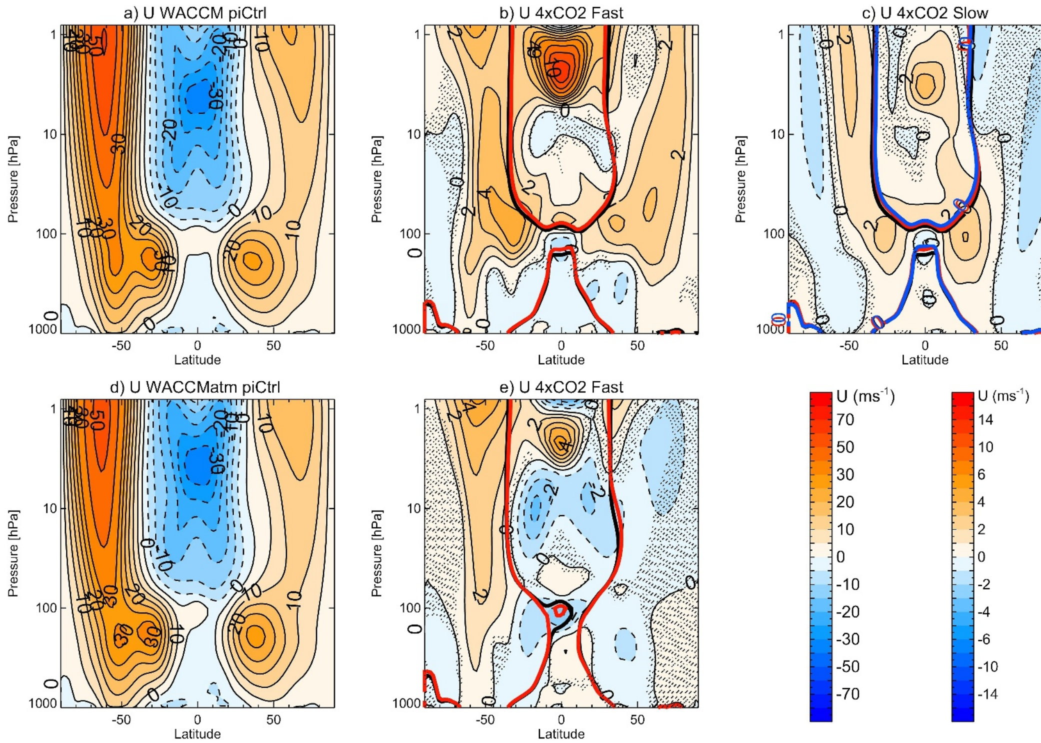


**Figure 4.** As in Figure 1 but for the zonal-mean zonal wind. The zero wind line is indicated in black for the piControl climatology, red for the climatology of the fast response (years 6–25) and blue for the total response (years 81–100). Contours are drawn every 5 m $s^{-1}$ for the climatologies and every 1 m $s^{-1}$ for the responses as indicated in the colorbars (left colorbar for the climatologies, right colorbar for the responses).

different waves. In the lower stratosphere, resolved waves in WACCM are the main driver of the shallow branch in the piControl climatology (78% at 100 hPa), with a smaller contribution from (parameterized) orographic gravity waves (12% at 100 hPa). Resolved waves in the model are also the main contributor to the fast and slow responses to 4x$CO_2$ in the lower stratosphere. The contribution of orographic gravity waves is negligible in the fast response while they account for about 25% of the slow response (note that in turn the slow response at 100 hPa is only about 25% of the total response, as shown in Figure 2).

The DCP states that the latitude-averaged value of $\overline{w}^*$ on a pressure level depends only on the difference in the vertically integrated wave drag between the edges of the averaging region (Haynes et al., 1991). The latitude-pressure distribution of the Eliassen Palm (EP) flux and its divergence is shown in Figure 7. The fast response (Figure 7b) clearly shows the enhancement of two regions of negative EP flux divergence in the subtropics in the lower stratosphere, centered at about 25N and 25S. These changes reinforce the climatological EP flux divergence and drive most of the fast response in tropical upwelling in the shallow branch. Enhanced EP flux divergence in this region is related to the intensification and upward extension of the subtropical jets, shown in Figure 4b, which is due to changes in the meridional temperature gradient in the upper troposphere-lower stratosphere region (Figure 5b). This mechanism seems to operate also in the slow response, although changes in the temperature gradient, subtropical jets and EP flux divergence are much smaller.

The very weak response in the subtropical jets in WACCMatm (Figure 4e), consistent with a more homogeneous latitudinal distribution of zonal mean temperature change (Figure 5e) is associated with a minimal response in the shallow branch (Figure 5e), in agreement with Figure 1e. Our results therefore corroborate the mechanism proposed in previous modeling studies to understand the climatological behavior of $\overline{w}^*$ and its response under increasing $CO_2$ in the shallow branch (e.g., Garcia & Randel, 2008; Shepherd & McLandress, 2011). Our analysis also provides additional information about the timing of the response and its driving mechanisms. We have shown

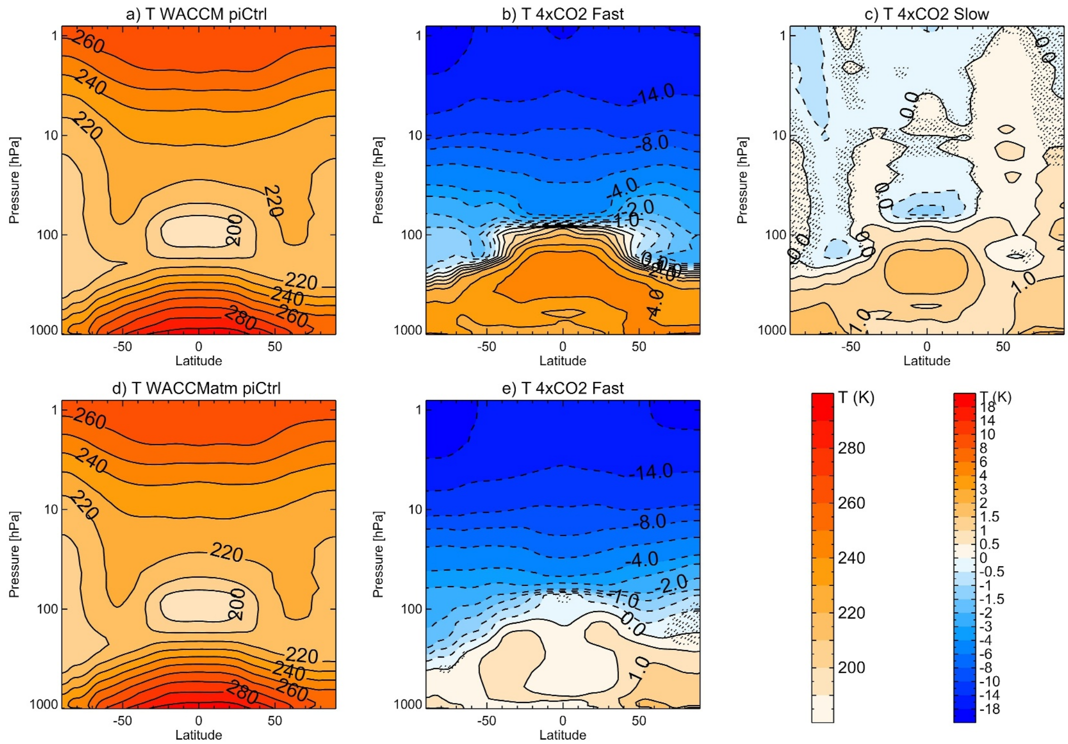


**Figure 5.** As in Figure 1 but for the zonal mean zonal temperature. Contours are drawn every 10 K for the climatologies (left colorbar). In the response, contour intervals vary as indicated in the right hand side colorbar.

that most of the response in resolved wave forcing driving the shallow branch occurs in the first 25 years after the 4xCO2 increase and is due to changes in the temperature of the well-mixed shallow ocean.

In the deep branch, according to the DCP, resolved waves are also the largest contributor to the WACCM piControl climatology of $\overline{w}^{*}$, with only a small contribution from parameterized gravity waves. In contrast, the response (both fast and slow) to abrupt 4x$CO_2$ forcing is dominated by non-orographic gravity waves (NOGW), mainly of frontal origin. Note that in WACCMatm, where tropical upwelling responds only to radiative adjustment, resolved waves are still the primary contributor, followed by NOGW. To understand these differences, we analyzed the spatial pattern of these responses in the wave drag for the major contributors, that is, resolved waves in the model and NOGW, shown in Figures 7 and 8, respectively.

First, we compare differences in resolved wave drag in the fast response in WACCM and WACCMatm. In WACCM, the fast response in the EP flux divergence (Figure 7b) is indicative of an upward displacement of the climatological pattern. As explained above, in the lower stratosphere enhanced propagation of resolved waves occurs toward the subtropics because of the intensification of the subtropical jets (Figure 3b). This is consistent with reduced Rossby wave propagation and dissipation at middle and polar latitudes in the middle and upper stratosphere (Figure 7b), and an intensification of the zonal mean zonal winds therein (Figure 4b). In contrast, in WACCMatm, resolved waves propagate more readily toward middle and high latitudes, dissipating in the middle and upper stratosphere mainly in the Northern Hemisphere, which reinforces the piControl climatological pattern in the NH. This is consistent with the lack of intensification of the subtropical jets in WACCMatm, a more homogeneous latitudinal structure of zonal mean T in the UTLS region and a much smaller warming of the troposphere compared to WACCM.

Figure 8 shows the climatological behavior and 4x$CO_2$ responses of NOGWD computed as the sum of non orographic gravity wave drag of frontal origin and convective origin. In all responses (Figures 8b, 8c, and 8e), the pattern in the upper stratosphere is opposite to the climatology. In the ocean-coupled WACCM ensemble,

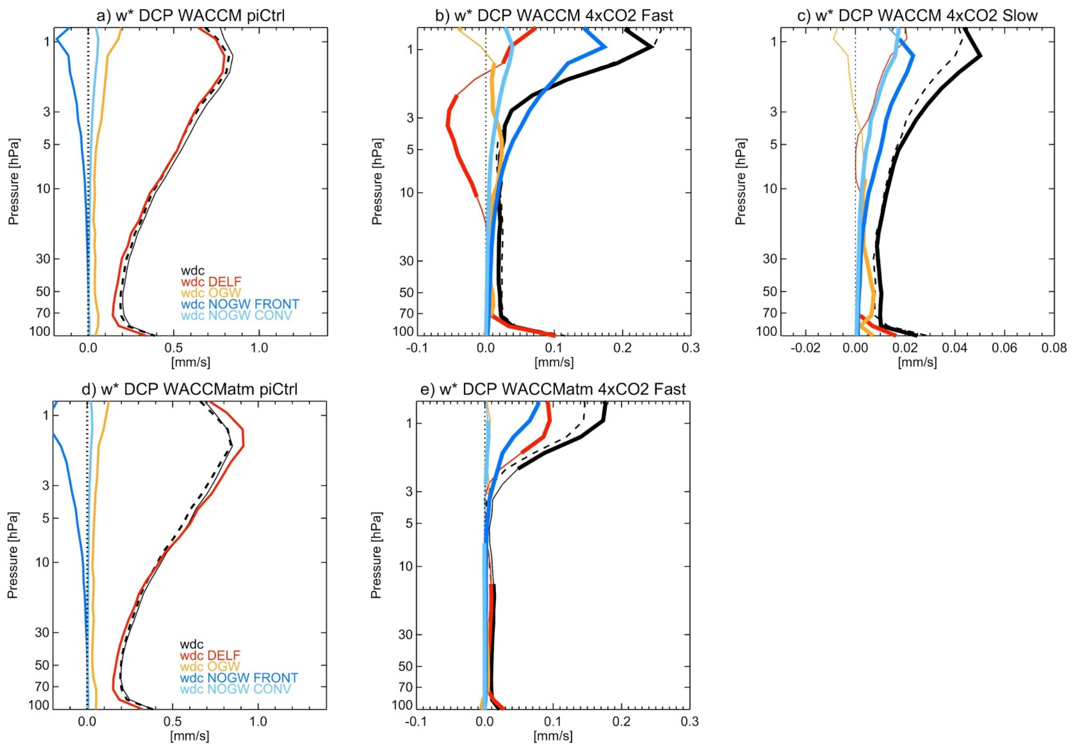


**Figure 6.** Vertical profile of $\overline{w}^*$ (mm/s) averaged between the piControl climatological TA latitudes. Dashed black indicates model output; solid black indicates the DCP calculations with all waves included. The DCP contribution of each type of wave to the tropical w* is denoted by the various colors DELF for resolved waves in the model, OGW for parameterized orographic gravity waves, NOGW FRONT for parameterized non orographic gravity waves of frontal origin, NOGW CONV for parameterized non orographic gravity waves of convective origin. The piControl climatology is shown in the left column, the fast response in the middle, and the slow response on the right. WACCM results are in the top row and WACCMatm in the bottom row. In the response, thick lines indicate the levels where the responses are significant according to a Student's *t*-test at the 95% confidence level.

NOGWD is larger in the subtropics than in WACCMatm and the negative values extend down to the middle stratosphere explaining the dominant contribution of NOGWs to the tropical mean (about 30N–30S) $\overline{w}^*$ response computed from the DCP. This larger response in WACCM compared to WACCMatm in the subtropics is mainly due to larger changes in the filtering of the westerly part of the spectrum of NOGWs at these latitudes (i.e., 20–30N and 20–30S, not shown) due to the fast response in the subtropical jets, which is not seen in WACCMatm (cf. Figures 4b and 4e). This mechanism is similar to the one that explained changes in the deep branch of the BDC in WACCM in different RCP scenarios (see Figure 10 in Palmeiro et al. (2014) and its discussion). A small reduction (about 10%, not shown) in NOGW sources of frontal origin also contributes to the total change in NOGWD in both fast and slow responses. Therefore, the intensification of the subtropical jets in WACCM forced by changes in the SSTs mainly leads to changes in the filtering of NOGW of frontal origin and drive most of the changes in the deep branch tropical upwelling at fast and slow timescales.

In summary, the strengthening and upward extension of the subtropical jets caused by warmer SSTs due to the concomitant enhancement of the meridional temperature gradient at the surface effectively modulate the filtering of NOGW of frontal origin. Further, the filtering effect explains the sizable contribution of these waves to the fast and slow response in the tropical upwelling in the upper stratosphere. Fast radiative adjustments, as seen in WACCMatm, can explain the contribution of resolved waves to the changes. Taken together, the comparison of the WACCM and WACCMatm responses in the upper stratosphere indicate that the contributions of forcings are not merely additive and that compensation (Sigmond & Shepherd, 2014) between resolved and gravity waves might be taking place.

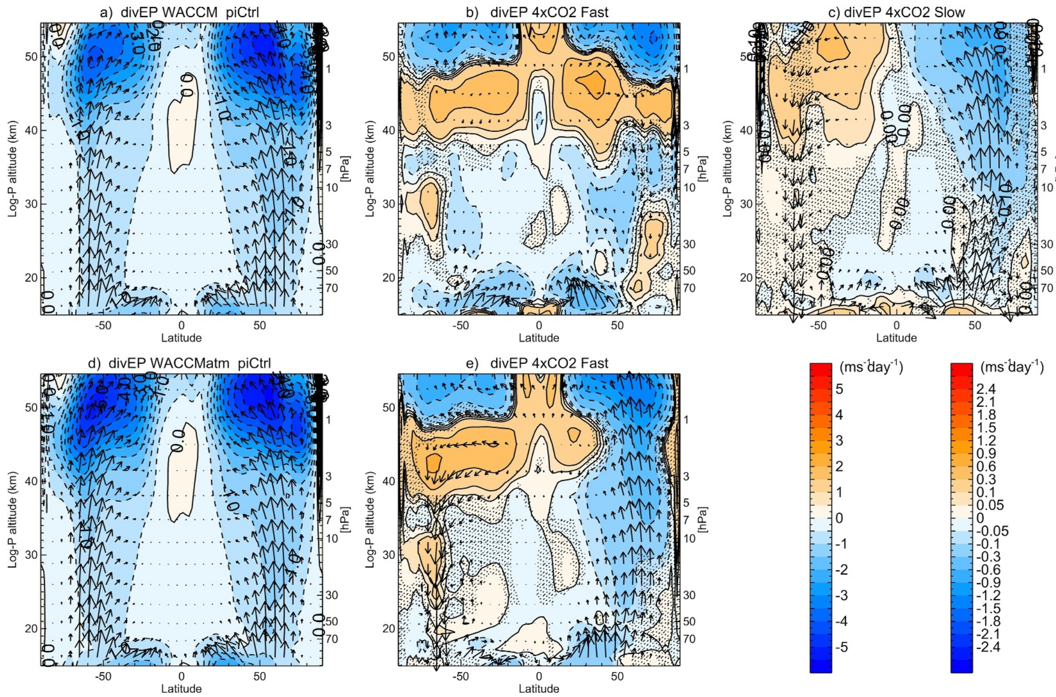


**Figure 7.** As in Figure 1 for the Eliassen-Palm flux (vectors) and its divergence (contours). Vertical and meridional components of EPflux have been multiplied by the square root of density for readability. Contours are drawn every 0.5 mm $s^{-1}$ for the climatologies and at 0, 0.05, 0.1, 0.3 mm $s^{-1}$ and every 0.3 mm $s^{-1}$ $day^{-1}$ therefater for the responses as indicated in the colorbars (left colorbar for the climatologies, right colorbar for the responses). Dotted areas denote non-significant values of the EP flux divergence response.

## 4. Discussion and Conclusions

We have investigated the timescales of the tropical upwelling response to an abrupt quadrupling of $CO_2$ in the shallow and deep branches of the BDC to understand the role of the different forcing agents, namely, the direct effect of rapid atmospheric adjustments (basically stratospheric cooling) versus the indirect effect of increasing SSTs. To do so, a three-member ensemble of transient simulations under an abrupt quadrupling of CO2 has been compared with a preindustrial control simulation carried out with the atmosphere-ocean coupled version of WACCM. Insofar as the influence of warming surface temperatures operates on both fast (shallow ocean) and slow (deep ocean) time scales, we have also attempted to discriminate between the effect of the warming shallow ocean and the atmospheric radiative adjustments from increased atmospheric $CO_2$. To do so, in addition to separating the fast and slow responses in WACCM, the coupled-ocean WACCM simulations were compared with simulations using the atmosphere-only version of WACCM (WACCMatm), with prescribed SSTs from a pre-industrial control run. Our conclusions are summarized below.

1. In the shallow branch of the BDC, most of the response to an abrupt quadrupling of CO2 occurs on fast timescales, that is, within the first couple of decades of the simulation. At 100 hPa, the fast response accounts for 77% of the final response. The comparison of the fast responses in simulations with and without a coupled ocean indicate that the fast response in w*is driven mainly by changes in the SSTs from the well mixed shallow ocean. The contribution of the rapid adjustments to CO2-driven stratospheric cooling is only about 10% of the total response in WACCM. Our results agree with previous modeling studies that highlighted the primary role of warmer SSTs in response to increasing CO2 in driving the changes of the shallow branch of the BDC (Abalos et al., 2021; Chrysanthou et al., 2020; Garny et al., 2011; Oberlander et al., 2013). However, to the best of our knowledge, our study is the first in which the rate of development of the response is quantified.

   The $\overline{w}^*$ response of the shallow branch is mainly due to stronger EP flux divergence from resolved waves in the model, consistent with an intensification and upward extension of the subtropical jets as proposed by Garcia and Randel (2008) and Shepherd and McLandress (2011). The analysis of timescales reveals that most of the

10.1029/2024JD041780

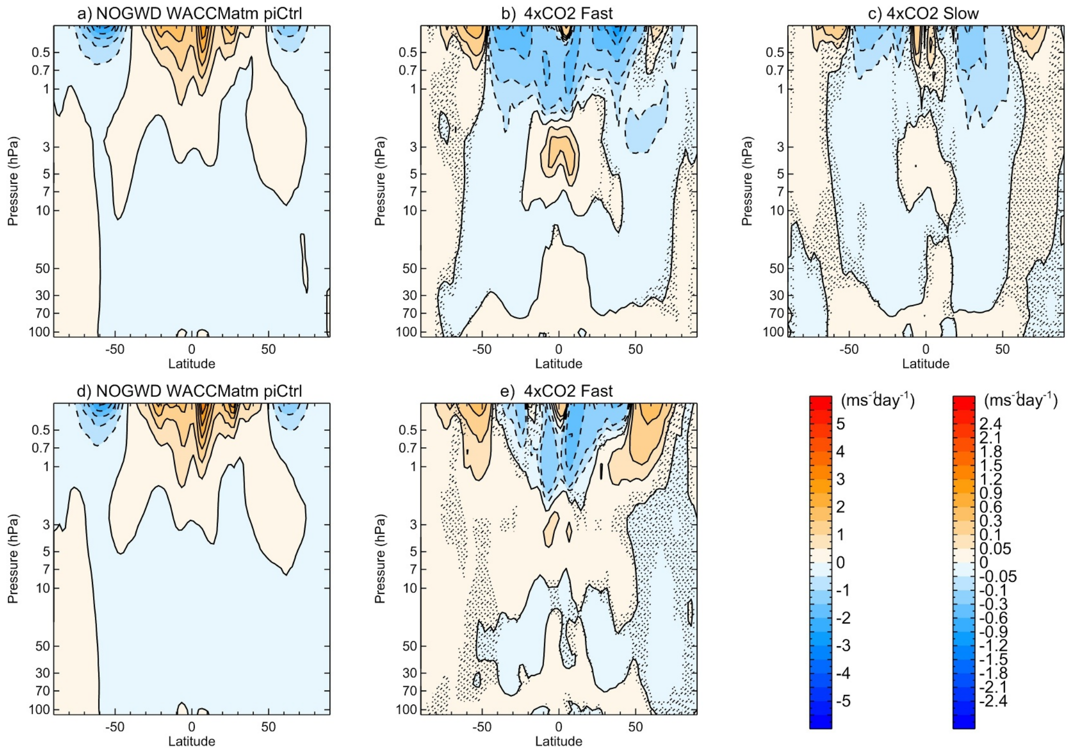


**Figure 8.** As in Figure 1 but for non-orographic gravity wave drag. Contours are drawn every 0.5 mm $s^{-1}$ $day^{-1}$ for the climatologies and at 0, 0.05, 0.1, 0.3 mm $s^{-1}$ $day^{-1}$ and every 0.3 mm $s^{-1}$ $day^{-1}$ therefater for the responses, as indicated in the colorbars (left colorbar for the climatologies, right colorbar for the responses). Dotted areas denote non-significant values of the EP flux divergence response.

enhanced forcing by Rossby waves occurs quickly and is related to changes in the meridional gradient of tropospheric temperature that follows the fast warming of the SSTs in the mixed layer ocean.

2. In the deep branch of the BDC, the intensification of the mean tropical upwelling in response to an abrupt quadrupling of $CO_2$ occurs earlier and develops more rapidly in the upper stratosphere than in the lower stratosphere. At 1 hPa, the fast response accounts for 86% of the total response, which indicates a faster behavior of the deep branch compared to the shallow branch (77% at 100 hPa) and a much smaller contribution of the slow response in the deep branch (14% vs. 23%, which is about 60% smaller). This faster behavior in the deep branch is due to the larger contribution of the direct radiative adjustments to increased $CO_2$, which cause changes in $\overline{w}^*$ in the upper stratosphere but not in the lower stratosphere. Indeed, we can quantify the contribution of each of the forcings to the fast response in WACCM: at 1 hPa, 70% of the increase in mean tropical upwelling is due to direct radiative adjustments from quadrupling $CO_2$ and only 30% is due to warmer SSTs. Furthermore, most of the effect of the rapid adjustment occurs already within the first year after the forcing and remains more or less constant afterward, while the influence of warmer SSTs steadily continues over longer timescales. This is why the contribution of the radiative adjustments and warmer SSTs to the final response (that at years 80–99) are almost equal (55% and 45% respectively, at 1 hPa).

Previous studies have quantified the contribution of the direct radiative forcing versus warmer SSTs in time slice simulations in atmosphere-only models, which do not account for atmosphere-ocean feedbacks (Chrysanthou et al., 2020; Oberlander et al., 2013). Their results are qualitatively similar to ours regarding the larger role of radiative adjustments in driving changes in the deep branch compared to the shallow branch. Oberlander et al. (2013) compared the BDC response under A1b GHG conditions in year 2095 with year 2000 in the EMAC model and found that about two thirds of the change in $\overline{w}^*$ in the upper stratosphere was due to radiative adjustments versus one third due to warmer SSTs. Chrysanthou et al. (2020) analyzed the BDC response upon quadrupling CO2 concentrations and reported an equal contribution of each forcing mechanism in the HadGEM3-A model. However, both studies are not directly comparable to ours. Oberlander et al. (2013) analyzed GHG scenarios, and both of them only examined the total (near-equilibrium) response without investigating the timescales over which it developed.

Finally, unlike the shallow branch, the deep branch responds to 4x$CO_2$ forcing in WACCM via changes in the filtering of non-orographic gravity waves (mainly of frontal origin) in the subtropics, following changes in the subtropical zonal mean zonal winds. This mechanism dominates in both fast and slow responses. In contrast, in atmosphere-only simulations with preindustrial SSTs (WACCMatm), aimed at isolating the direct effect of radiative cooling from $CO_2$, changes in the subtropical jets in the lower stratosphere are minimal and enhanced convergence from resolved waves explain most of the changes in tropical upwelling in the upper stratosphere.

The simulations in this study are highly idealized, by design, since our goal was to separate the different mechanisms that lead to an acceleration of the BDC under increased $CO_2$ forcing. However, if one wishes to carefully quantify how the BDC will evolve in coming decades, transient forcing scenarios will be needed. Not only because $CO_2$ increases gradually, but because other anthropogenic forcings affect the BDC in important ways. Notably, ozone depleting substances (ODS) have contributed to accelerating the BDC in the second half of the 20$^{th}$ century and, as a consequence of the Montreal Protocol, will oppose the effects of increasing $CO_2$ and decelerate the BDC in the coming decades (Abalos et al., 2019; Polvani et al., 2018, 2019). Also, since those substances crucially control the levels of stratospheric ozone, and since ozone abundance controls stratospheric temperature and thus the stratospheric circulation, it would be important to carefully examine the role of ozone recovery in future BDC changes. This is a complex task since stratospheric ozone, which is expected to increase with the phasing out of ODS, is also sensitive to $CO_2$ (see, e.g., Chiodo et al., 2018), which cools the stratosphere thus affecting stratospheric chemistry. $CO_2$ also affects ozone by accelerating the BDC itself, which transports ozone from the tropics to the poles at high levels. In this study the effects of ozone changes due to the 4x$CO_2$ increase are simulated in WACCM, but we have not separated them out. In addition, our simulations do not include an internally generated QBO; changes in the QBO with increasing CO2 (e.g., a decrease in amplitude, Richter et al., 2020) would also feed back on the BDC response shown here. Thus, disentangling the effects of stratospheric ozone and the QBO, and quantifying the relative importance of $CO_2$ and ODS, are complex tasks. New specifically designed simulations—with single forcings, and with and without interactive atmospheric chemistry—will be needed to document in full detail all the mechanisms in play.

## Data Availability Statement

The WACCM data used for the analysis in this study are freely available at: https://doi.org/10.3929/ethz-b-000677011.

**Acknowledgments**
The National Center for Atmospheric Research (NCAR) is sponsored by the U.S. National Science Foundation (NSF). Computing resources were provided by NCAR's Climate Simulation Laboratory, sponsored by NSF and other agencies. This research was enabled by the computational and storage resources of NCAR's Computational and Information Systems Laboratory (CISL). NC acknowledges support from the project RecO3very: PID2021-12477OB-I00 from the Spanish Ministry of Science and Innovation and also acknowledges support from NCAR through its Affiliate Scientist Programme. RRG was supported in part by NASA Grant 80NSSC19K1214. G.C. was partly supported by the Swiss National Science Foundation via the Ambizione Grant PZ00P2_180043 and via the Simons Foundation Grant MPS-MP-SRM-00005208. LMP is funded, in part, by an award from the US National Science Foundation to Columbia University.

## References

Abalos, M., Calvo, N., Benito-Barca, S., Garny, H., Hardiman, S. C., Lin, P., et al. (2021). The Brewer-Dobson circulation in CMIP6 models. *Atmospheric Chemistry and Physics Chemistry and Physics*, *21*(17), 13571–13591. https://doi.org/10.5194/acp-21-13571-2021

Ábalos, M., Polvani, L., Calvo, N., Kinnison, D., Ploeger, F., Randel, W., & Solomon, S. (2019). New insights on the impact of ozone depleting substances in the Brewer-Dobson circulation. *Journal of Geophysical Research - Atmospheres*, *124*, 2435–2451. https://doi.org/10.1029/2018JD029301

Albers, J. R., Perlwitz, J., Butler, A. H., Birner, T., Kiladis, G. N., Lawrence, Z. D., et al. (2018). Mechanisms governing interannual variability of stratosphere-to- troposphere ozone transport. *Journal of Geophysical Research-Atmosphere*, *123*(1), 234–260. https://doi.org/10.1029/2017JD026890

Arblaster, J. M., Gillett, N. P., Calvo, N., Foster, P. M., Polvani, L. M., Son, S.-W., et al. (2014). Stratospheric ozone changes and climate. In *Chapter 4 in scientific assessment of ozone depletion, global ozone research and monitoring project, report No. 55*. World Meteorological Organization.

Birner, T., & Bönisch, H. (2011). Residual circulation trajectories and transit times into the extratropical lowermost stratosphere. *Atmospheric Chemistry and Physics*, *11*(2), 817–827. https://doi.org/10.5194/acp-11-817-2011

Brewer, A. W. (1949). Evidence for a world circulation provided by the measurements of helium and water vapour distribution in the stratosphere. *Quaterly Journal of the Royal Meteorological Society*, *95*, 213–243.

Butchart, N. (2014). The Brewer- Dobson circulation. *Reviews of Geophysics*, *52*(2), 157–184. https://doi.org/10.1002/2013RG000448

Butchart, N., & Perez-Charlton, A. (2010). Chapter 4 in stratospheric dynamics. In V. Eyring, T. Shepherd, & D. Waugh (Eds.), *SPARC report on evaluation of chemistry – climate models*. SPARC Report No. 5, WCRP-132, WMO/TD-No.1526.

Calvo, N., & Garcia, R. R. (2009). Wave forcing of the tropical upwelling in the lower stratosphere under increasing concentrations of greenhouse gases. *Journal of the Atmospheric Sciences*, *66*(10), 3184–3196. https://doi.org/10.1175/2009JAS3085.1

Ceppi, P., Zappa, G., & Shepherd, T. G. (2018). Fast and Slow components of the extratropical atmospheric circulation response to $CO_2$ forcing. *Journal of Climate*, *31*(3), 1091–1105. https://doi.org/10.1175/JCLI-D-17-0323.1

Chiodo, G., Polvani, L. M., Marsh, D. R., Stenke, A., Ball, W., Rozanov, E., et al. (2018). The response of the ozone layer to quadruple $CO_2$ concentrations. *Journal of Climate*, *31*(10), 3893–3907. https://doi.org/10.1175/JCLI-D-17-0492.1

Chrysanthou, A., Maycock, A. C., & Chipperfield, M. P. (2020). Decomposing the response of the stratospheric Brewer-Dobson circulation to an abrupt quadrupling in CO2. *Weather Climate Dynamics*, *1*, 155–174. https://doi.org/10.5194/wcd-1-155-2020

Deckert, R., & Dameris, M. (2008). Higher tropical SSTs strengthen the tropical upwelling via deep convection. *Geophysical Research Letters*, *35*(10), L10813. https://doi.org/10.1029/2008GL033719

Dessler, A. E., Schoeberl, M. R., Wang, T., Davis, S. M., & Rosenlof, K. H. (2013). Stratospheric water vapor feedback. *PNAS*, *110*(45), 18087–18091. https://doi.org/10.1073/pnas.1310344110

Dobson, G. M. B. (1956). Origin and distribution of the polyatomic molecules in the atmosphere. *Proceedings of the Royal Society of London*, *236*, 187–193.

Garcia, R. R., & Randel, W. J. (2008). Acceleration of the Brewer–Dobson circulation due to increases in greenhouse gases. *Journal of the Atmospheric Sciences*, *65*(8), 2731–2739. https://doi.org/10.1175/2008JAS2712.1

Garny, H., Dameris, M., Randel, W. J., Bodeker, G. E., & Deckert, R. (2011). Dynamically forced increase of tropical upwelling in the lower stratosphere. *Journal of the Atmospheric Sciences*, *68*(6), 1214–1223. https://doi.org/10.1175/2011JAS3701.1

Garny, H., Hendon, H., Abalos, M., Chiodo, G., Purich, A., Randel, W. J., et al. (2022). *Stratospheric ozone changes and climate, chapter 5 in scientific assessment of ozone depletion, GAW Report No. 278*. World Meteorological Organization.

Grise, K., & Polvani, L. M. (2017). Understanding the time scales of the tropospheric circulation response to abrupt CO2 forcing in the Southern Hemisphere: Seasonality and the Role of the Stratosphere. *Journal of Climate*, *30*(21), 8497–8515. https://doi.org/10.1175/JCLI-D-16-0849.1

Hall, T. M., & Plumb, R. A. (1994). Age as diagnostic of stratospheric transport. *Journal of Geophysical Research*, *99*(D1), 1059–1070. https://doi.org/10.1029/93JD03192

Hardiman, S., Butchart, N., & Calvo, N. (2013). The morphology of the Brewer-Dobson circulation and its response to climate change in CMIP5 simulations. *Quaterly Journal of the Royal Meteorological Society*, *140*(683), 1958–1965. https://doi.org/10.1002/gj.2258

Hardiman, S. C., Butchart, N., & Calvo, N. (2014). The morphology of the Brewer-Dobson circulation and its response to climate change in CMIP5 simulations. *Quaterly Journal of the Royal Meteorological Society*, *140*(683), 1958–1965. https://doi.org/10.1002/qj.2258

Haynes, P. H., Marks, C. J., McIntyre, M. E., Shepherd, T. G., & Shine, K. P. (1991). On the “downward control” of extratropical diabatic circulations by eddy-induced mean zonal forces. *Journal of the Atmospheric Sciences*, *48*(4), 651–680. https://doi.org/10.1175/1520-0469(1991)048<0651:OTCOED>2.0CO;2

Karpechko, A., Yu, A. C., Abalos, M., Akiyoshi, H., Arblaster, J. M., Garfinkel, C. I., et al. (2018). Stratospheric ozone changes and climate. In *Chapter 5 in scientific assessment of ozone depletion: Global ozone research and monitoring project, report No. 58*. World Meteorological Organization.

Kinnison, D. E., Brasseur, G. P., Walters, S., Garcia, R. R., Marsh, D. R., Sassi, F., et al. (2007). Sensitivity of chemical tracers to meteorological parameters in the MOZART-3 chemical transport model. *Journal of Geophysical Research*, *112*(D20), D20302. https://doi.org/10.1029/2006JD007879

Li, F., Stolarski, R. S., Pawson, S., Newman, P. A., & Waugh, D. (2010). Narrowing of the upwelling branch of the Brewer-Dobson circulation and Hadley cell in chemistry-climate model simulations of the 21st century. *Geophysical Research Letters*, *37*(13), L13702. https://doi.org/10.1029/2010GL043718

Lin, P., & Fu, Q. (2013). Changes in various branches of the Brewer-Dobson circulation from an ensemble of chemistry climate models. *Journal of Geophysical Research: Atmospheres*, *118*(1), 73–84. https://doi.org/10.1029/2012JD018813

Marsh, D. R., Mills, M. J., Kinnison, D. E., Lamarque, J.-F., Calvo, N., & Polvani, L. M. (2013). Climate change from 1850 to 2005 simulated in CESM1(WACCM). *Journal of Climate*, *26*(19), 7372–7391. https://doi.org/10.1175/JCLI-D-12-00558.1

Menzel, M. E., Waugh, D. W., & Orbe, C. (2023). Connections between upper troposphere and lower stratospheric circulation responses to increase $CO_2$. *Journal of Climate*, *36*(12), 4101–4112. https://doi.org/10.1175/JCLI-D-22-0851.1

Oberlander, S., Langematz, U., & Meul, S. (2013). Unraveling impact factors for future changes in the Brewer-Dobson circulation. *Journal of Geophysical Research*, *118*(18), 10296–10312. https://doi.org/10.1002/jgrd.50775

Olsen, M. A., Shoeberl, M. R., & Nielsen, J. E. (2007). Response of stratospheric circulation and stratosphere-troposphere exchange to changing sea surface temperatures. *Journal of Geophysical Research*, *112*(D16), D16104. https://doi.org/10.1029/2006JD008012

Oman, L., Waugh, D. W., Pawson, S., Stolarski, R. S., & Newman, P. A. (2009). On the influence of anthropogenic forcings on changes in the stratospheric mean age. *Journal of Geophysical Research – Atmosphere*, *114*(D3), 1–15. https://doi.org/10.1029/2008JD010378

Palmeiro, F. M., Calvo, N., & Garcia, R. R. (2014). Future changes in the Brewer–Dobson circulation under different greenhouse gas concentrations in WACCM4. *Journal of the Atmospheric Sciences*, *71*(8), 2962–2975. https://doi.org/10.1175/JAS-D-13-0289.1

Plumb, R. A. (2002). Stratospheric transport. *Journal of the Meteorological Society of Japan*, *80*(4B), 793–809. https://doi.org/10.2151/jmsj.80.793

Polvani, L. M., Abalos, M., Garcia, R., Kinnison, D., & Randel, W. J. (2018). Significant weakening of Brewer-Dobson circulation trends over the 21st century as a consequence of the Montreal Protocol. *Geophysical Research Letters*, *45*(1), 401–409. https://doi.org/10.1002/2017GL075345

Polvani, L. M., Wang, L., Abalos, M., Butchart, N., Chipperfield, M. P., Dameris, M., et al. (2019). Large impacts, past and future, of ozone-depleting substances on Brewer-Dobson circulation trends: A multi-model assessment. *Journal of Geophysical Research*, *124*(13), 6669–6680. https://doi.org/10.1029/2018JD029516

Rayner, N. A., Parker, D. E., Horton, E. B., Folland, C. K., Alexander, L. V., Rowel, D. P., et al. (2003). Global analysis of sea surface temperature, sea ice and night marine air temperature since the late nineteenth century. *Journal of Geophysical Research*, *108*(D14), 4407. https://doi.org/10.1029/2002JD002670

Richter, J., Butchart, N., Kawatani, Y., Bushell, A. C., Holt, L., Serva, F., et al. (2020). Response of the Quasi Biennial Oscillation to a warming climate in global climate models. *Quaterly Journal of the Royal Meteorological Society*, *148*(744), 1490–1518. https://doi.org/10.1002/qj.3749

Shepherd, T. G., & McLandress, C. (2011). A robust mechanism for strengthening of the Brewer–Dobson circulation in response to climate change: Critical-layer control of subtropical wave breaking. *Journal of the Atmospheric Sciences*, *68*(4), 784–797. https://doi.org/10.1175/2010JAS3608.1

Sigmond, M., & Shepherd, T. G. (2014). Compensation between resolved wave driving and parameterized orographic gravity wave driving of the Brewer-Dobson circulation and its response to climate change. *Journal of Climate*, *27*(14), 5601–5610. https://doi.org/10.1175/JCLI-D-13-00644.1

10.1029/2024JD041780


Sigmond, M., Siegmund, P. C., Manzini, E., & Kelder, H. (2004). A simulation of the separate climate effects of middle atmospheric and tropospheric CO2 doubling. *Journal of Climate*, *17*(12), 2352–2367. https://doi.org/10.1175/1520-0442(2004)017<2352:asotsc>2.0.co;2

Taylor, K. E., Stouffer, R. J., & Meehl, G. A. (2012). An overview of CMIP5 and the experiment design. *Bulletin of the American Meteorological Society*, *93*(4), 485–498. https://doi.org/10.1175/BAMS-D-11-00094.I

Yang, H., & Zhu, J. (2011). Equilibrium thermal response timescale of global oceans. *Geophysical Research Letters*, *38*(14), L14711. https://doi.org/10.1029/2011GL048076